J Mater Sci (2009) 44:3662–3673
DOI 10.1007/s10853-009-3489-5

Synthesis, characterization and thermal analysis of Fe-doped boehmite nanofibres and nanosheets

Yanyan Zhao · Jing Yang · Ray L. Frost · János Kristóf · Erzsébet Horváth

Received: 29 August 2008 / Accepted: 11 April 2009 / Published online: 11 May 2009

Abstract It is important that one should have knowledge of the thermal stability of synthesized nanomaterials. In this research, thermal analyses of both dynamic and controlled rate thermal analysis (CRTA) combined with infrared emission spectroscopy have been used to determine the thermal stability of iron-doped boehmite. Iron-doped boehmite nanofibres with varying iron contents have been prepared at low temperature using hydrothermal treatment in the presence of non-ionic poly (ethylene oxide) surfactant. The TEM images show that the resulting nanostructures are predominantly nanofibres when Fe doping is less than 5%; in contrast, nanosheets are the dominant for 10% Fe-doped boehmite. No nanofibre was observed in the case of 20% Fe-doped boehmite, instead, nanotubes, nanosheets and iron-rich nanoparticles were formed. Both dynamic thermal analysis and CRTA show that Fe-doped boehmite nanomaterials dehydroxylate at higher temperatures than pure boehmite nanofibres. In general, the higher the doped Fe %, the higher the dehydroxylation temperature. The dehydroxylation temperature indicated in the infrared emission spectroscopy of doped boehmite nanomaterials is in harmony with those in other thermal analysis studies.

Y. Zhao · J. Yang · R. L. Frost (✉)
Inorganic Materials Research Program, School of Physical and Chemical Sciences, Queensland University of Technology, 2 George Street, GPO Box 2434, Brisbane, QLD 4001, Australia
e-mail: r.frost@qut.edu.au

J. Kristóf
Department of Analytical Chemistry, University of Pannonia, P.O. Box 158, 8201 Veszprém, Hungary

E. Horváth
Department of Environmental Engineering and Chemical Technology, University of Pannonia, P.O. Box 158, 8201 Veszprém, Hungary

Introduction

In recent years, synthesis of inorganic materials on the nanoscale with special morphologies has been shown to be of great significance in material science [1, 2]. The intrinsic properties of nanoscale materials are mainly determined by their composition, structure, crystallinity, size and morphology [3]. In particular, one-dimensional (1D) nanoscale inorganic materials including nanofibers, nanowires and nanotubes have attracted intensive interest due to their distinctive geometries, novel physical and chemical properties, and potential applications in many areas [4–10].

Because of the high surface area, chemical and thermally stable properties and mesoporous properties, various alumina phases have been extensively used as carriers and supports for a variety of catalysts operating at both high and low temperatures. Alumina can be employed as catalyst [11], adsorbent [12, 13], composite materials [14, 15] and ceramics [16–18]. Boehmite (γ-AlOOH), a principal oxo-hydroxide of aluminium, can be used as building units and directing templates in the preparation of core/shell materials [16, 19]. Boehmite nanofibres were first synthesized by John Bugosh in 1961 [20]. Boehmite is also a crucial precursor in sol–gel technique for preparing high-purity and high-strength monolithic α-alumina ceramics for use as substrates for electronic circuits, abrasive grains, high-temperature refractory materials, fibres and thin films [21]. Since the resulting alumina

prepared from boehmite can keep the original size and morphology after calcination, great efforts have been devoted to the investigation of nanoscale boehmite materials, especially 1D nanostructures, such as nanofibres and nanotubes [22, 23].

Recently, Zhu et al. [24] reported an interesting new synthesis method in which a surfactant was used. Rather than acting as templates for the synthesis of mesoporous materials, the surfactant was able to direct formation of boehmite fibres [23]. It was also reported that a much higher Al concentration and lower temperatures can be used in this method compared to those used in traditional methods for the synthesis of boehmite nanofibres. This is an efficient approach of producing nanofibres in large quantity. The growth of boehmite nanofibres can be improved through a supply of fresh precipitate of aluminium hydrate at regular intervals, and the fibres can grow to over 100 nm in length under well-controlled reaction conditions. It is well known that the necessity of catalyst or absorbent separation later is an important problem in industrial catalytic process and water treatment. Apart from filtration technique, magnetic separation is another good method [25, 26]. In order to achieve magnetic property, doping with iron would be an ideal way. Besides, when doped with iron, the resulting boehmite nanostructure may have special optical properties which will enable it to be used for further industrial applications.

The synthesis of 1D boehmite nanostructures has been attracting much attention since a long time due to its unique properties and the potential for broad applications in industries as mentioned above. A variety of 1D boehmite nanostructures including nanofibers [27], nanotubes [27], nanorods [28] and nanobelts [28] were successfully prepared under different hydrothermal conditions at temperatures in the range of 100–180 °C in the past few years. In order to ensure the good quality including the morphology, size and enhanced property of the resultant Fe-doped 1D boehmite nanostructures, it is crucial and also the first step is to design a simple and efficient synthesis route.

Considering the energy efficiency and the resultant properties of the final products, we are aiming to produce iron-doped boehmite nanostructures with medium size and high crystallinity under a relatively low hydrothermal temperature. Zhu et al. [27] studied the synthesis of boehmite by adding $NaAlO_2$ solution into acetic acid solution and hydrothermally treating at 100 °C and reported that no nanofibres but irregular-shaped particles were formed without surfactant PEO at a PEO/Metal ion ratio of 0.47, whereas lath-shaped nanofibres, with a length over 50 nm and a constant thickness of about 3 nm were formed after 2 days of hydrothermal treatment. Zhu's result indicates that the use of PEO is important in order to achieve the desired 1D boehmite nanostructures. We mimicked this process and tried adding NaOH solution into Al $(NO_3)_3$ solution and hydrothermally treating at similar conditions with and without PEO [6]. It showed that boehmite nanotubes were formed with and without the presence of surfactant PEO after 2 days of hydrothermal treatment at 100 °C with an average length of about 100 nm. The morphology and size of the resultant nanotube products had a similar length and width as that of nanofibres prepared by Zhu's group, which enable these tubes exhibit much higher surface areas than fibres. Kuang et al. [22] fabricated boehmite nanotubes in the presence of a cationic surfactant CTAB through hydrothermal treatment at 120 °C. The typical length of the nanotubes prepared by Kuang et al. was in the range of 30–70 nm with the inner and outer diameter in the range of 3–4 nm and 5–6 nm, respectively. The preparation of large nanobelts and nanorods was also reported [28, 29] at a high temperature of 180 °C. A higher hydrothermal temperature normally can improve the growth rate of crystals and form crystals with high crystallinity. Zhu et al. [27] found a novel boehmite nanofibre synthesis approach where a regular supply of a fresh precipitate of aluminium hydroxide during hydrothermal treatment at 100 °C with a PEO-to-metal ion ratio of 0.4:1. Through this approach, it was reported that a rapid growth rate of boehmite fibers was achieved. Zhu et al. [27] proposed that the fresh precipitates of aluminum hydroxide act as a resource of building blocks attaching to the both ends of the existing fibres under the assistance of surfactant PEO to elongate fibres. On the basis of the above information, we choose to prepare Fe-doped 1D boehmite nanostructures through Zhu's novel synthesis approach at a hydrothemal temperature of 120 °C using Al $(NO_3)_3$ and NaOH as starting materials.

This study is a follow-up on the iron-doped boehmite study. The detailed characterization and discussion of phase, morphology and composition of the resultant nanostructures were reported in our earlier study [8]. The main focus of this study is the thermal analysis and infrared spectroscopy of the iron-doped nanostructures. Brief summary and discussion on the morphology and phase are presented at first to help understand the thermal analysis applied and infrared spectroscopy results. There have been very few studies underlying the importance of the thermal stability of nanomaterials. In this study, boehmite nanofibres based on the low temperature and soft chemical methodology were synthesized by introducing iron as dopant, and a series of iron-doped boehmite nanofibres with varying iron contents has been systematically studied using a combination of thermal analysis and infrared emission spectroscopy.

Experimental

Synthesis of Fe-doped boehmite nanofibres

A total amount of 0.25 mol aluminium nitrate and ferric nitrate were mixed before being dissolved in ultra-pure water. In order to make a comparison, mixtures with iron molar percentage of 0, 1, 2, 3, 4, 5, 10 and 20% were prepared separately and then dissolved in ultra-pure water to form solution with a metal ion-to-H_2O molar ratio of 1:100 and heated to 80 °C. A 5 mol L^{-1} NaOH solution was then added drop-wise at a constant rate of 5 mL min^{-1} to form precipitate. Then, it was aged for 3 h with constant stirring at 80 °C, the resulting precipitate was recovered by centrifugation, washed with pure water four times to remove sodium nitrate. The fresh precipitate was then split into five parts evenly for hydrothermal treatment and characterization. Water and non-ionic PEO surfactant Tergitol 15-S-7 ($C_{12-14}H_{25-29}O$ $(CH_2CH_2O)_7H$, Aldrich) with average molecular weight of $\sim$508 were mixed with the first part of precipitate at a metal:PEO:H_2O molar ratio of 1:0.4:16. The viscous mixture was stirred for 1 h at room temperature and then transferred into an autoclave and kept in oven at 120 °C. The remaining three parts of fresh precipitate and the same amount of ultra-pure water were added into autoclave every two days. Accordingly, the molar ratio of metal:PEO:H_2O changed to 2:0.4:32; 3:0.4:48 and 4:0.4:64, respectively, after 2, 4 and 6 days. The final product was washed with water first and then acetone and dried in air at 80 °C.

X-ray diffraction

The XRD analyses were performed on a PANalytical X'Pert PRO X-ray diffractometer (radius: 240.0 mm). Incident X-ray radiation was produced from a line-focused PW3373/10 Cu X-ray tube, operating at 45 kV and 35 mA, providing $K\alpha_1$ wavelength of 1.540596 Å. The incident beam passed through a 0.04 rad Soller slit, a ½° divergence slit, a 15-mm fixed mask and a 1° fixed anti-scatter slit. After interaction with the sample, the diffracted beam was detected by an X'Celerator RTMS detector. The detector was set in scanning mode, with an active length of 2.022 mm. Samples were analysed utilising Bragg-Brentano geometry over a range of 3–75° 2θ with a step size of 0.02° 2θ, with each step measured for 200 s.

Thermal analysis

Dynamic experiment Thermal decomposition of the iron-doped boehmite samples was carried out in a Derivatograph PC-type thermoanalytical instrument (Hungarian Optical Works, Budapest, Hungary) with the thermoanalytical equipment being capable of recording the thermogravimetric (TG), derivative thermogravimetric (DTG) and differential thermal analysis (DTA) curves simultaneously. The sample was heated in a ceramic crucible in static air atmosphere at a rate of 5 °C min^{-1}.

Controlled rate thermal analysis experiment Thermal decomposition of the iron-doped boehmite samples was carried out in a Derivatograph in a flowing air atmosphere (250 cm^3 min^{-1}) at a pre-set, constant decomposition rate of 0.15 °C min^{-1}. (Below this threshold value the samples were heated under dynamic conditions at a uniform rate of 0.1 °C min^{-1}.) The samples were heated in an open ceramic crucible at a rate of 0.1 °C min^{-1}. Using the quasi-isothermal, quasi-isobaric heating program of the instrument, the furnace temperature was regulated precisely to provide a uniform rate of decomposition in the main decomposition stage.

Infrared spectroscopy

Infrared spectra were obtained using a Nicolet Nexus 870 FTIR spectrometer with a smart endurance single bounce diamond ATR cell. Spectra over the 4000–525 cm^{-1} range were obtained by the co-addition of 64 scans with a resolution of 4 cm^{-1} and a mirror velocity of 0.6329 cm s^{-1}. Spectral manipulation such as baseline adjustment, smoothing and normalisation was performed using the GRAMS® software package (Galactic Industries Corporation, Salem, NH, USA).

Infrared emission spectroscopy

A FTIR emission spectroscopy was carried out on a Nicolet Nexus 870 FTIR spectrometer equipped with a TGS detector, which was modified by replacing the IR source with an emission cell. A description of the cell and principles of the emission experiment have been published elsewhere [30–33]. Approximately 0.2 mg of sample was spread as a thin layer (approximately 0.2 microns) on a 6-mm diameter platinum surface and held in an inert atmosphere within a nitrogen-purged cell during heating.

Band component analysis was undertaken using the Jandel 'Peakfit' (Erkrath, Germany) software package which enabled the selection of the type of fitting function and allowed specific parameters to be fixed or varied accordingly. Band fitting was done using a Lorentz–Gauss cross-product function with the minimum number of component bands used for the fitting process. The Lorentz–Gauss ratio was maintained at values greater than 0.7 and fitting was undertaken until reproducible results were obtained with squared correlations (r^2) greater than 0.995.

Band fitting of the spectra is quite reliable providing that there is some band separation or changes in the spectral profile.

Results and discussion

Transmission electron microscopy

All the resultant samples were identified as boehmite. Typical TEM images for the undoped and Fe-doped boehmites after 8 days of hydrothermal treatment at 120 °C with regular supply of fresh precipitate of Fe-doped aluminium hydroxide are shown in Fig. 1. When the pure boehmite was hydrothermally treated at a lower temperature of 100 °C with all the other conditions remaining the same, nanotubes were formed [8]. Boehmite nanotubes doped with gallium were also achieved via a similar hydrothermal route at 100 °C [7]. However, when the treated temperature was increased to 120 °C, as can be seen in Fig. 1, the characteristic morphology of boehmite prepared with and without Fe doping is of lathlike nanofibres. Interestingly, the morphology of boehmite was nanofibres doped with yttrium when treated at the same hydrothermal conditions at 100 °C [34]. The morphology change indicates hydrothermal temperature, and dopants play an important role in the morphology and growth of boehmite crystal. As shown in Fig. 1, nanofibres are dominant in synthesized boehmite samples with the doped Fe percentage no more than 5%. The morphology and size of Fe-doped nanofibres with doped Fe percentage in the range of 1–5% are very much similar; therefore, only 3% and 5% Fe-doped boehmites were presented in Fig. 1. As expected, the higher hydrothermal temperature resulted in the formation of much longer boehmite nanostructures. Pure nanofibres with lengths up to 300 nm were synthesized, which is around two times longer than that reported in a previous study where boehmite nanofibres were prepared at a lower temperature of 100 °C [6]. The resultant Fe-doped boehmite nanofibres prepared at 120 °C were overall shorter than the pure boehmite nanofibres that were prepared under the same conditions, but remarkably longer than those pure boehmite nanofibres/nanotubes synthesized at 100 °C. Both nanosheets and nanofibres were observed in 10% Fe-doped sample where nanosheets with beveled ends were dominant. Instead of forming nanofibres, nanotubes as well as nanosheets and iron-rich phase were formed. Based on EDX analysis conducted in our previous study [8], only a limited amount of Fe substituted Al in the boehmite nanostructures. A linear relationship between added % Fe and actual % Fe for samples after ageing but before hydrothermal treatment was observed in the range of 1–20% doped Fe. However, a miscibility gap occurred after 8 days of treatment showing the maximum aluminium that can be substituted by iron is about 4.4%.

The mechanism of the growth of boehmite nanotubes at 100 °C in the presence of the nonionic surfactant PEO has been systematically investigated [6, 8]. It was proposed that the initially formed 1D nanotubes after 2 days of hydrothermal treatment at 100 °C with PEO being firstly attached to the surface of PEO micelles through hydrogen bonding; then the tiny nanotubes, the so-called building units, growing along the micelles; that the growth rate slowed down or even ceased when the length of the nanotube was approaching towards the total length of the directing micelle. However, the growth of boehmite nanostructures at 120 °C with PEO cannot be interpreted through the above mechanism. An obvious reason for the same is that the length of PEO micelles decreases with the increase in temperature [35, 36] whereas the resultant nanofibres were much longer than the expected length of PEO micelles. This result suggested that at a higher temperature (120 °C), PEO is not the key factor for the growth of boehmite 1D nanostructures. It was reported that relatively large boehmite nanorods can be achieved at a high temperature of 180 °C without any surfactant under a similar hydrothermal conditions using the same starting materials [29, 34], which also show that surfactant is not crucial for the growth of boehmite nanostructures at relatively high temperatures. It is well known that Oswald ripening occurs during crystal growth where small particles with a critical radius r_c are present. If $r < r_c$, the particle grows; if $r > r_c$, the particle shrinks; and r_c is determined by the experimental conditions [37]. It can be proposed that the growth of boehmite nanofibres under 120 °C is controlled by the Oswald ripening process. In the process of boehmite growth, the PEO micelles may act as templates which interact with those tiny doped boehmite nanocrystallites forming longer 1D nanostructures. A supplementary experiment for the synthesis of undoped or doped boehmites should be performed at 120 °C without surfactant PEO for further comparison. Even if PEO surfactant had little effect on the formation of doped boehmite nanofibres, it can be expected that there would be a higher surface area of alumina prepared with surfactant due to the large amount of micro- and mesopores generated by PEO after calcination.

X-ray diffraction

The X-ray diffraction patterns of the hydrothermally treated boehmite are shown in Fig. 2. The XRD patterns show the precipitates to be boehmite γ-AlOOH except for a minor amount of bayerite formed in 0% and 1% samples. In accordance with the Debye–Scherrer equation, the crystallite sizes vary initially from 15.5 nm in pure boehmite, to a constant value of $\sim$22 nm with Fe doping. The XRD peaks in the patterns for 1% Fe-doped boehmite

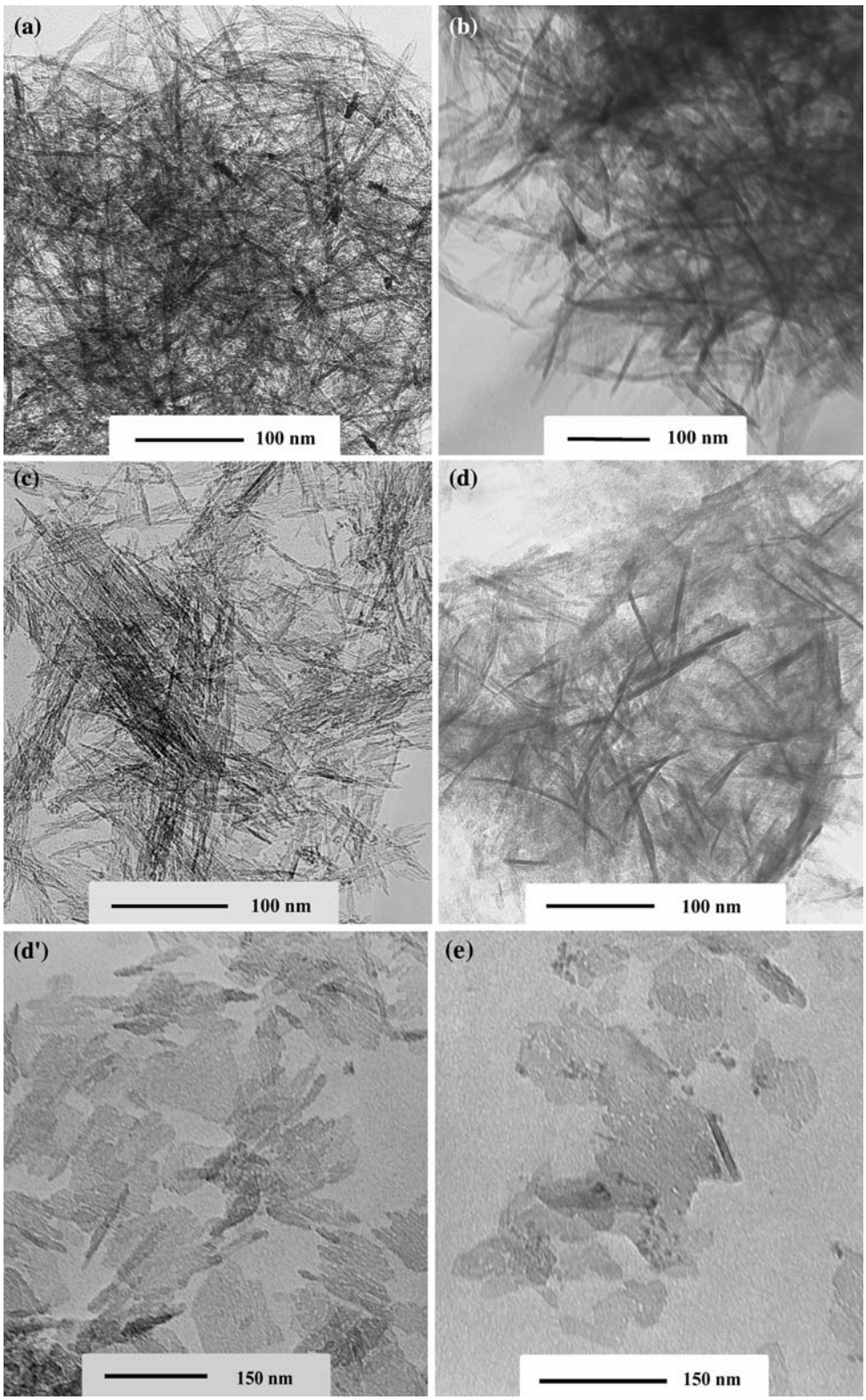

Fig. 1 TEM images of **a** pure boehmite, **b** 3% Fe, **c** 5% Fe, **d** and **d′** 10% Fe, **e** 20% Fe-doped boehmite nanostructures prepared at 120 °C after 8 days of hydrothermal treatment

nanostructures show decreased peak width with the increase in hydrothermal time, indicating a gradual increase in crystallinity of the nanostructures during the soft chemical treatment. Compared to boehmite prepared at 100 °C, a remarkably larger crystallite size at 120 °C, which is about 20% larger, was observed. The larger crystallite size could partially contribute to the formation of longer fibres.

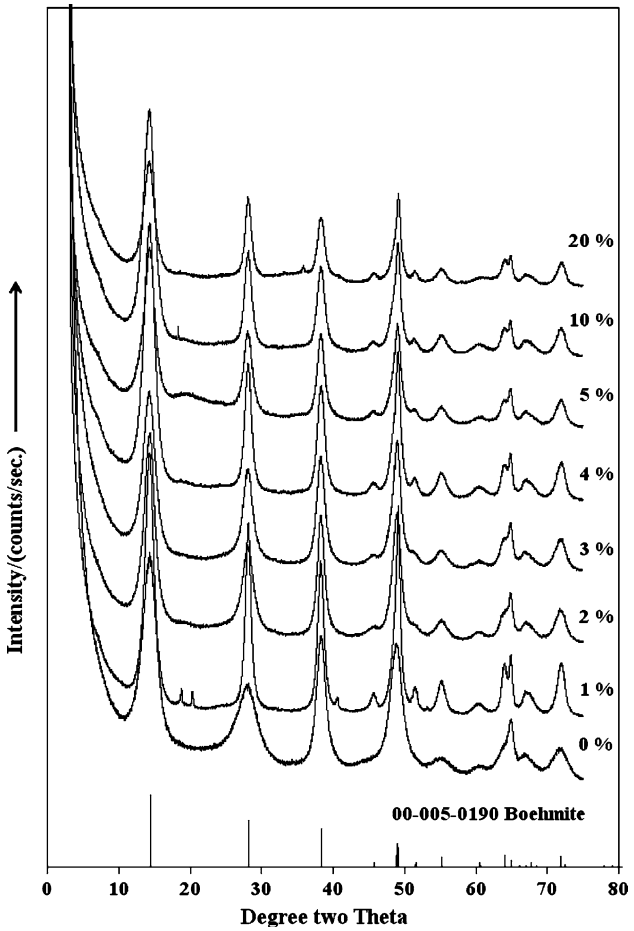

Fig. 2 X-ray diffraction patterns of boehmite, and 1, 2, 3, 4, 5, 10 and 20% Fe doped boehmite

Thermal analysis

The study of the thermal stability of materials is of importance for our understanding of nanomaterials. One method of studying the thermal stability is to undertake thermal analysis experiments. There are several methodologies for thermal analysis, which can be used. Two of such experiments, namely the first one is the so-called dynamic experiment in which the nanomaterial is heated at a constant rate, and the second experiment involves controlling the heating rate according to the mass loss. This latter technique is called CRTA or the controlled rate thermal analysis.

The dynamic experiment

In the dynamic experiment a constant heating rate is employed to determine the temperatures of mass losses. The dynamic thermal analyses of the boehmite and Fe-doped boehmite are shown in Fig. 2a–f. The results of the

Table 1 Decomposition stages under dynamic conditions for Fe-doped boehmites

Sample: Boehmite 1% Fe doped			Sample: Boehmite 3% Fe doped			Sample: Boehmite 5% Fe doped			Sample: Boehmite 10% Fe doped			Sample: Boehmite 20% Fe doped		
Temperature range (°C)	Mass loss (Sample mass: 61.79 mg)		Temperature range (°C)	Mass loss (Sample mass: 62.65 mg)		Temperature range (°C)	Mass loss (Sample mass: 116.16 mg)		Temperature range (°C)	Mass loss (Sample mass: 67.96 mg)		Temperature range (°C)	Mass loss (Sample mass: 121.78 mg)	
	mg	%		mg	%		mg	%		mg	%		mg	%
25–166	2.6	4.2	30–191	4.3	6.9	26–134	5.6	4.8	24–155	2.4	3.5	27–176	5.8	4.8
						134–181	3.5	3.0	155–219	1.2	1.8	176–278	4.1	3.4
166–279	1.2	1.9	191–370	6.6	10.5	181–291	15.6	13.4	219–286	3.5	5.2			
279–500	8.5	13.8				291–521	21.6	18.6	286–360	3.7	5.4	279–356	4.7	3.9
			370–495	4.8	7.7				360–509	6.5	9.6	356–511	11.6	9.5
500–884	1.1	1.8	495–865	1.0	1.6	521–800	1.1	0.9	509–894	1.0	1.5	511–866	1.8	1.5

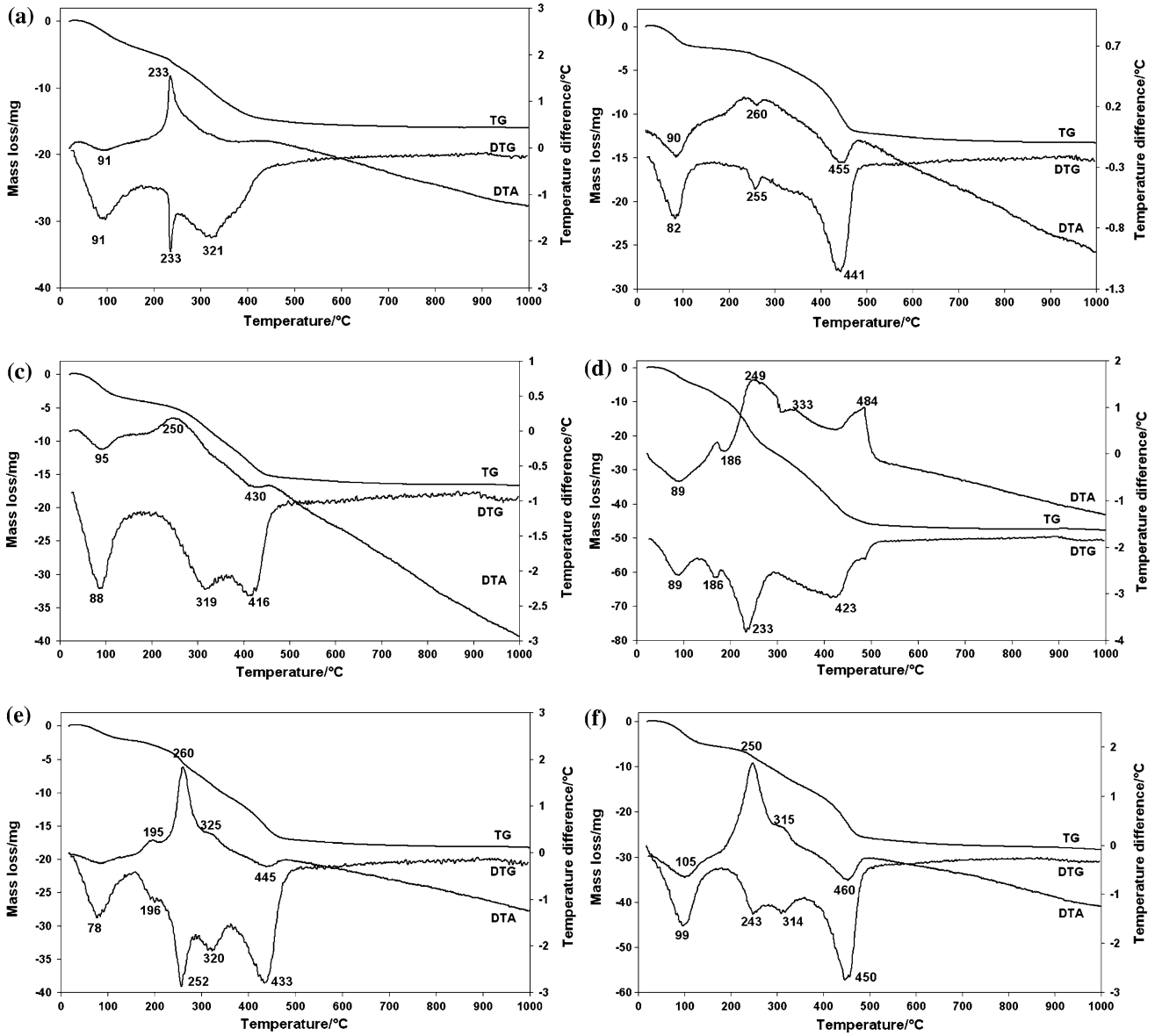

Fig. 3 Dynamic thermal analysis of **a** boehmite and **b** 1%, **c** 3%, **d** 5%, **e** 10%, **f** 20% Fe-doped boehmite

calculations shown in the Appendix are reported in Table 1.

Pure synthesized boehmite shows three decomposition steps. The step which is characteristic of boehmite is the sharp DTG step at 321 °C with a mass loss of 17.1%. The first mass loss occurs at around 91 °C with a mass loss of 9.0%. This mass loss step is attributed to the loss of adsorbed water. The second mass loss step is observed at around 233 °C and accounts for the major mass loss step with 4.8% mass loss. The third mass loss step occurs at 321 °C. This mass loss is attributed to interstitial water trapped between the boehmite layers. The theoretical mass loss based upon the equation $2AlOOH \rightarrow Al_2O_3 + H_2O$ is 11.5%. A large exotherm is observed in the DTA pattern at 233 °C and is attributed to the enthalpy required for the combustion of the surfactant used in the synthesis of boehmite.

The DTG pattern for the 1% Fe-doped boehmite (Fig. 3b) shows three mass loss steps at 82, 255 and 441 °C. There are three endothermic peaks observed at 90, 260 and 455 °C. The mass loses are 4.2, 1.9 and 13.8% over the temperature ranges 25–166, 166–279 and 279–500 °C, respectively. By comparison of the thermal analysis patterns for pure synthetic boehmite and 1% Fe-doped boehmite, the effect of the Fe doping is to raise the temperature of dehydroxylation of the boehmite quite significantly from 321 °C to 441 °C. Transmission electron microscopy of the boehmite and the 1, 3 and 5% doped

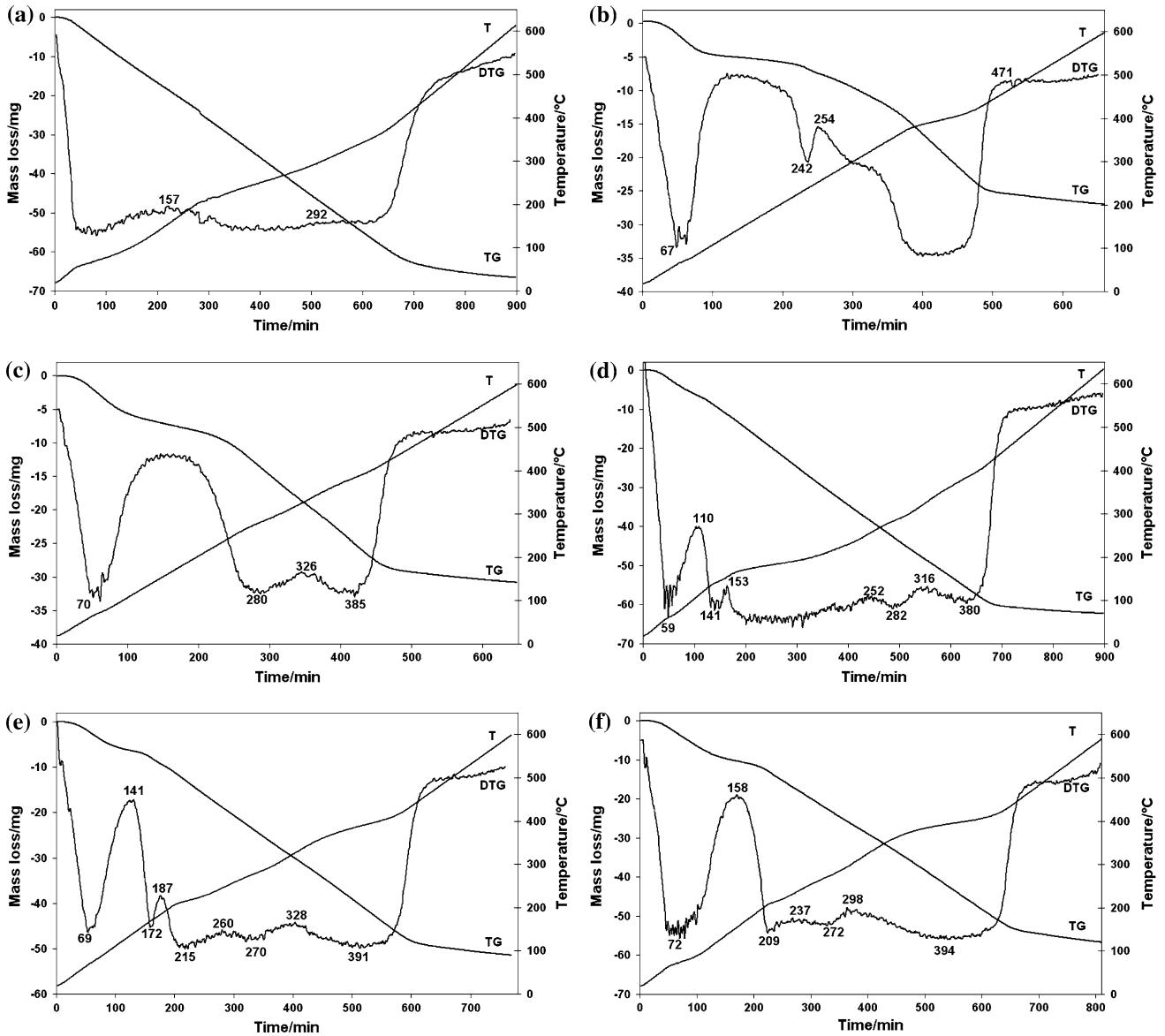

Fig. 4 Controlled rate thermal analysis of **a** boehmite and **b** 1%, **c** 3%, **d** 5%, **e** 10%, **f** 20% Fe-doped boehmite

boehmite shows that the materials consist only of nanofibres. Thus, this thermal analysis pattern for the 1% Fe-doped boehmite is that of a Fe-doped boehmite nanofibre.

This effect of increase in dehydroxylation temperature is also observed for the 3% doped boehmite (Fig. 3c). The temperature of dehydroxylation has increased to 416 °C. Three peaks in the DTG curve are observed at 88, 319 and 416 °C. Three peaks are also observed in the DTA pattern with endotherms at 95 and 430 °C and an exotherm at 250 °C. These enthalpy changes are associated with (a) the loss of adsorbed water (b) dehydroxylation of boehmite and (c) combustion of the surfactant. For the 3% Fe-doped boehmite, mass losses that are observed in the 30–191, 191–370, 370–495 and 495–865 °C temperature ranges are 6.9, 10.5, 7.7 and 1.6%, respectively (Table 1). This temperature dehydroxylation increase is also observed for the 5% doped boehmite (Fig. 3d). The temperature of dehydroxylation has increased to 423 °C. Four DTG peaks are observed at 89, 186, 233 and 423 °C. For the 5% Fe-doped boehmite mass losses that are observed in the 26–134, 134–181, 181–291, 291–521 and 521–800 °C temperature ranges are 4.8, 3.0, 13.4, 18.6 and 0.9%, respectively. The DTA pattern shows greater complexity. DTA peaks are observed at 89, 186, 249, 333 and 484 °C. These enthalpy changes are assigned to (a) water desorption, (b) goethite dehydroxylation, (c) combustion of the surfactant and (d) boehmite dehydroxylation.

As the % of doping is increased, the number of mass loss steps increases. For the 10% Fe-doped boehmite, five mass loss steps are observed at 78, 196, 252, 320 and

433 °C (Fig. 3e). There is a strong exothermic peak at 260 °C. It is proposed that this peak is due to the combustion of the surfactant. The number of DTG steps is associated with an increased number of phases. As the concentration of Fe is increased, the hydrothermally treated boehmite becomes a mixture of nanofibres and nanosheets. These peaks are possibly attributable to (a) first decomposition step to goethite (b) the decomposition of the surfactant and (c) decomposition step to boehmite nanosheets. The DTG pattern of the 20% Fe-doped boehmite is similar to that of the 10% Fe-doped boehmite. Five mass loss steps are observed at 99, 243, 314 and 450 °C with mass losses of 4.8, 3.4, 3.9, 9.5 and 1.5%.

The controlled rate thermal analysis experiment

The thermal analysis of the synthetic boehmite and Fe-doped boehmite under controlled CRTA conditions are shown in Fig. 4a–f. The results of the calculations shown in the Appendix are reported in Table 2. The CRTA result for boehmite synthesized at 120 °C is shown in Fig. 4a. Two pseudo-isothermal steps at 60 °C and 292 °C are observed and are attributed to dehydration and dehydroxylation of boehmite.

The CRTA of the 1% doped boehmite displays significant differences to that of the pure boehmite. The DTG curve for the 1% Fe-doped boehmite shows peaks at 67, 242 and 423 °C (Fig. 4b). This latter mass loss occurs as an isothermal step. These mass loss steps are ascribed to dehydration, loss of surfactant and dehydroxylation of the boehmite. The DTG curve for the 3% Fe-doped boehmite shows peaks at 70, 280 and 385 °C (Fig. 4c). None of these steps appears to be isothermal. The DTG curve in the CRTA experiment for the 5% doped boehmite appears different from the 1% and 3% doped boehmite curves. Peaks are observed at 59, 141, 282 and 380 °C. It is noted that after 153 °C, there is almost a continuous mass loss. The CRTA of 10% and 20% Fe-doped boehmite sample display four steps which are in harmony with the dynamic experiments. The DTG curve for 10% Fe-doped boehmite shows peaks at 69, 172, 215, 270, 391 °C. Peaks at 72, 209, 272 and 394 °C were observed for 20% Fe-doped boehmite.

Infrared emission spectroscopy

The infrared emission spectra of the 5% and 10% Fe-doped boehmite in the 700–1700 cm^{-1} region are shown in Fig. 5a and b and in the 2700–3900 cm^{-1} region in Fig. 6a and b. These figures show the change in intensity of the infrared bands as a function of temperature. The infrared absorption spectra of boehmite γ-AlOOH shows two bands

Table 2 Decomposition stages under CRTA conditions for Fe-doped boehmites

Sample: Boehmite 1% Fe doped			Sample: Boehmite 3% Fe doped			Sample: Boehmite 5% Fe doped			Sample: Boehmite 10% Fe doped			Sample: Boehmite 20% Fe doped		
Temperature range (°C)	Mass loss (Sample mass: 129.84 mg)		Temperature range (°C)	Mass loss (Sample mass: 118.64 mg)		Temperature range (°C)	Mass loss (Sample mass: 153.16 mg)		Temperature range (°C)	Mass loss (Sample mass: 194.62 mg)		Temperature range (°C)	Mass loss (Sample mass: 260.87 mg)	
	mg	%		mg	%		mg	%		mg	%		mg	%
22–129	5.3	4.1	22–166	7.4	6.2	21–110	6.5	4.2	21–141	6.5	3.3	22–158	10.5	4.0
						110–153	4.7	3.1	141–187	3.0	1.5	158–237	7.3	2.8
129–254	2.6	2.0	166–326	11.4	9.6	153–252	26.9	17.6	187–260	11.6	6.0			
254–471	18.0	13.9				252–316	9.3	6.1	260–328	9.3	4.8	237–298	8.5	3.3
			326–462	10.6	8.9	316–452	13.1	8.6	328–476	19.2	9.9	298–471	28.0	10.7
471–595	1.4	1.1	462–593	1.4	1.2	452–628	1.7	1.1	476–595	1.8	0.9	471–595	2.6	1.0

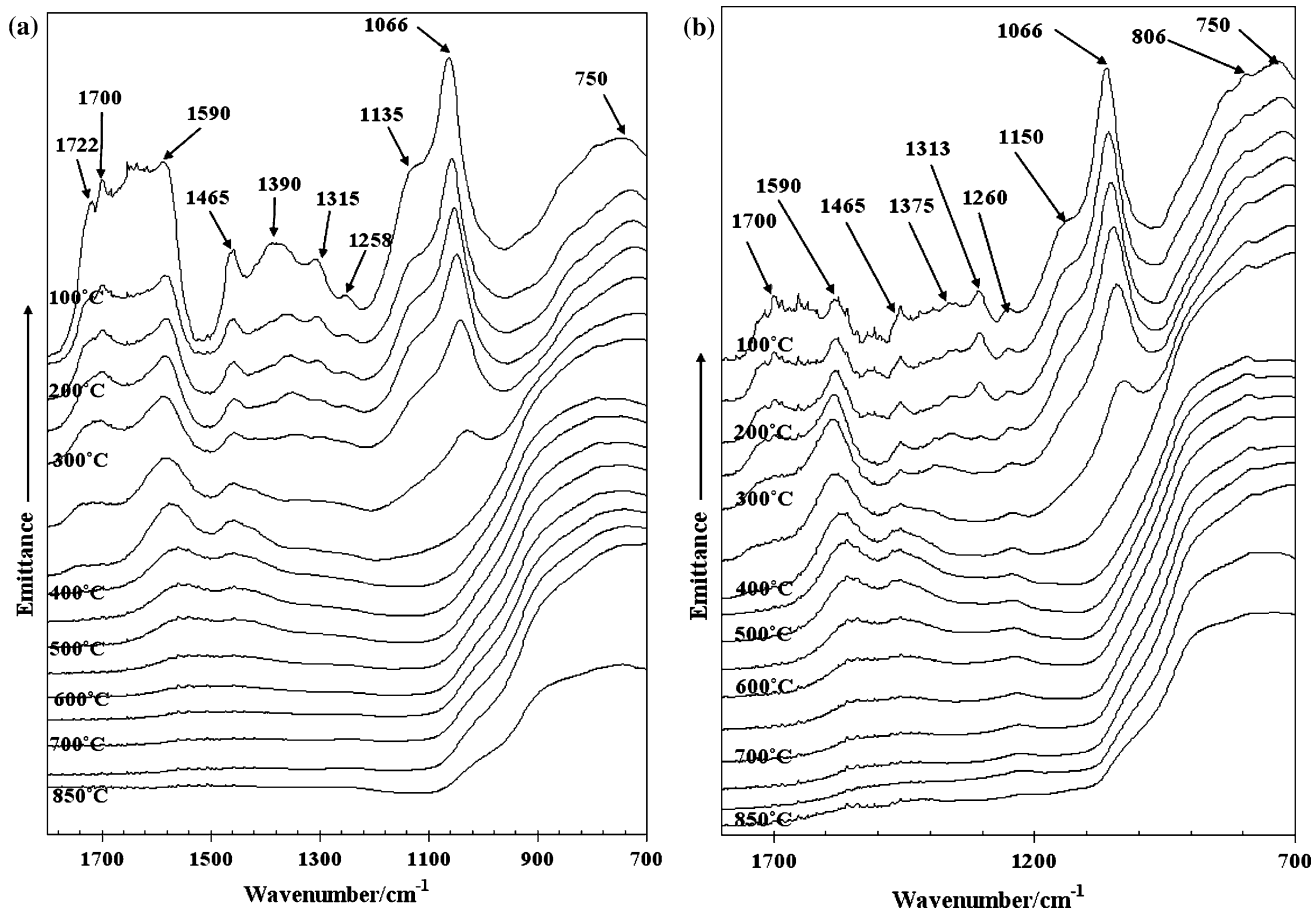

Fig. 5 Infrared emission spectra of **a** 5% and **b** 10% Fe-doped boehmite in the 700–1700 cm^{-1} region

at 3090 cm^{-1} and 3297 cm^{-1} assigned to the OH stretching vibrations of boehmite and at 1080 cm^{-1} and 1160 cm^{-1} assigned to δOH deformation modes. In Fig. 5a, infrared bands are observed at 1066 cm^{-1} and 1135 cm^{-1} which are assigned to the δOH deformation modes. The intensity of these two bands decreases until no intensity remains by 350 °C. This temperature in the infrared emission spectra indicates the temperature of dehydroxylation. The value is in agreement with the thermal analysis studies. The bands at 750 cm^{-1} and 860 cm^{-1} are ascribed to OAlO vibrations. Other infrared bands are observed at 1258, 1315, 1390 and 1465 cm^{-1}. These bands are attributed to overtone and combination bands which can be commonly observed in the infrared emission spectra. It is noted that the intensity of these bands is also lost by 350 °C.

For the 10% Fe-doped boehmite, the infrared bands are observed at 1066 cm^{-1} and 1150 cm^{-1} and as before are assigned to the δOH deformation modes. The intensity of these bands approaches zero by 350 °C. The two bands at 750 cm^{-1} and 806 cm^{-1} attributed to OAlO stretching vibrations appear to be retained until quite high temperatures, e.g. ~700 °C.

The infrared emission spectra in the OH stretching region show two bands at 3140 cm^{-1} and 3340 cm^{-1} ascribed to the boehmite OH stretching vibrations as well as bands at 2867, 2933 and 2967 cm^{-1} attributed to CH stretching vibrations of the templating surfactant. The intensity of both sets of bands diminishes as the temperature is raised. No intensity in these bands remains by 450 °C. In the infrared emission spectra of the 10% Fe-doped boehmite, two bands at 3125 cm^{-1} and 3350 cm^{-1}, assigned to the boehmite OH stretching vibrations, show no intensity by 450 °C. The positions of these bands suggest that the OH units of boehmite are strongly hydrogen bonded. An additional band at 3669 cm^{-1} is observed and assigned to free or non-hydrogen bonded OH units of the boehmite.

Conclusions

Fe-doped boehmite nanofibres ~250 nm in length with varying widths and nanosheets have been prepared at 120 °C using soft chemical hydrothermal methodology

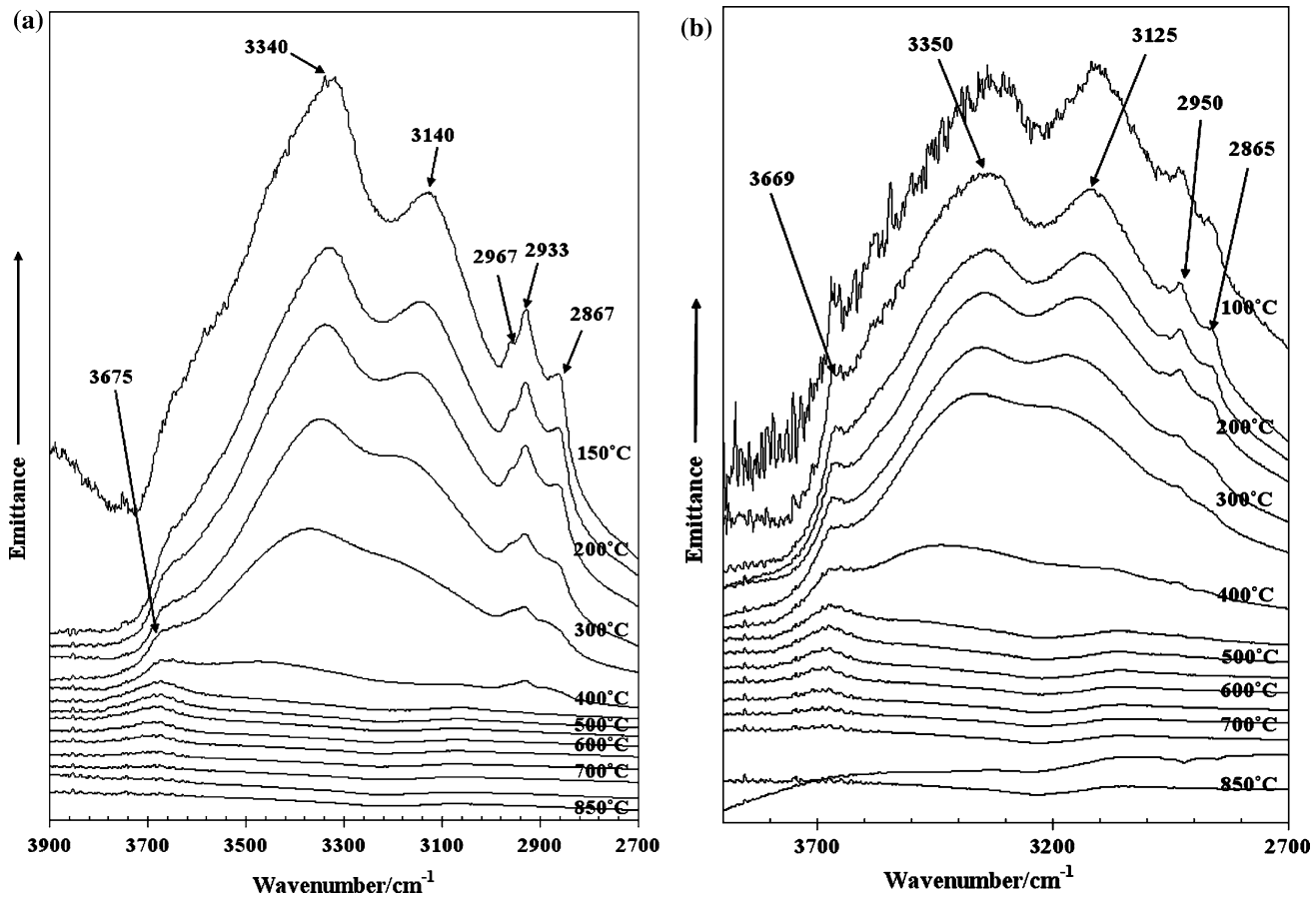

Fig. 6 Infrared emission spectra of **a** 5% and **b** 10% Fe-doped boehmite in the 2700–3900 cm^{-1} region

using PEO as a surfactant directing agent. In comparison with the pure boehmite nanostructures prepared at the same condition, the doped Fe has little effect on the morphology and size of the resultant nanostructures when the doped Fe% is less than 5%; whereas the doped Fe has significant influence on the growth of boehmite nanostructures when the doped Fe% is no less than 10%. Fibres or needles were formed at low Fe-doped samples. With the increasing iron content nanosheets are formed. Nanotubes were formed when added Fe content is increased to 20%.

At low doped Fe%, the dynamic thermal analysis of the Fe-doped boehmite nanofibres shows three decomposition steps which are assigned to dehydration, dehydroxylation of boehmite and further dehydroxylation. At high doped Fe%, as the % of Fe doping is increased, the number of mass losses steps increases due to the increased number of phases formed, which is in agreement with TEM results. For the Fe-doped boehmite with Fe concentration above 5%, the thermal decomposition is of a mixed system consisting of both boehmite nanofibres and boehmite nanosheets. The relatively sharp DTG steps at the range of 320–450 are characteristic of doped boehmite. Compared to pure boehmite nanostructures, Fe-doped boehmite nanostructures dehydroxylate at remarkably higher temperatures. It is also noted that there is an obvious gradual increase in dehydroxylation temperature with the increase in the doped Fe% from 2% to 20%.

The infrared emission spectra show bands at 1066 cm^{-1} and 1150 cm^{-1} for 5% Fe-doped boehmite, bands at 1066 cm^{-1} and 1150 cm^{-1} for 10% Fe-doped boehmite which can be assigned to the δOH deformation modes. The intensity of these bands approaching zero by 350 °C indicates the temperature of dehydroxylation. The value obtained by infrared emission spectra is in agreement with the thermal analysis studies.

Acknowledgements The financial and infrastructure support of the Queensland University of Technology Inorganic Materials Research Program of the School of Physical and Chemical Sciences is gratefully acknowledged. The authors thank The Australian Research Council (ARC) for funding the Thermal Analysis facility through a LIEF grant. One of the authors (YZ)owes his gratitude for a Queensland University of Technology international doctoral scholarship (QIDS).

Appendix

$AlO(OH) \cdot xH_2O \rightarrow AlO(OH) + xH_2O$

Calculation of water content for Fe-doped boehmite using the formula $AlO(OH) \cdot xH_2O$

(A) 1% Fe-doped boehmite

Composition: $AlO(OH) \cdot xH_2O$
Loss of water up to 129 °C is 5.3 mg (0.294 mmol)
Mass of dehydrated mineral is 124.54 mg (2.076 mmol)
Thus, the amount of crystallization water is 0.14 mol.

(B) 3% Fe-doped boehmite

Composition: $AlO(OH) \cdot xH_2O$
Loss of water up to 166 °C is 7.4 mg (0.411 mmol)
Mass of dehydrated mineral is 111.24 mg (1.854 mmol)
Thus, the amount of crystallization water is 0.22 mol.

(C) 5% Fe-doped boehmite

Composition: $AlO(OH) \cdot xH_2O$
Loss of water up to 110 °C is 6.5 mg (0.361 mmol)
Mass of dehydrated mineral is 146.66 mg (2.444 mmol)
Thus, the amount of crystallization water is 0.15 mol.

(D) 10% Fe-doped boehmite

Composition: $AlO(OH) \cdot xH_2O$
Loss of water up to 141 °C is 6.5 mg (0.361 mmol)
Mass of dehydrated mineral is 188.12 mg (3.135 mmol)
Thus, the amount of crystallization water is 0.12 mol.

(E) 20% Fe-doped boehmite

Composition: $AlO(OH) \cdot xH_2O$
Loss of water up to 158 °C is 10.5 mg (0.583 mmol)
Mass of dehydrated mineral is 250.37 mg (4.173 mmol)
Thus, the amount of crystallization water is 0.14 mol.

References

1. Fendler JH, Meldrum FC (1995) Adv Mater (Weinheim, Germany) 7:607
2. Lakshmi BB, Patrissi CJ, Martin CR (1997) Chem Mater 9:2544
3. Sun Y, Xia Y (2002) Nature 298:2176
4. Zhao Y, Frost RL, Martens WN, Zhu HY (2007) J Therm Anal Calorim 90:755
5. Zhao Y, Frost RL, Martens WN (2007) J Phys Chem C 111:16290
6. Zhao Y, Frost RL, Martens WN, Zhu HY (2007) Langmuir 23:9850
7. Zhao Y, Frost RL, Martens WN (2007) J Phys Chem C 111:5313
8. Zhao Y, Martens WN, Bostrom TE, Zhu HY, Frost RL (2007) Langmuir 23:2110
9. Zhao Y, Frost RL, Yang J, Martens WN (2008) J Phys Chem C 112:3568
10. Gudiksen MS, Lauhon LJ, Wang J, Smith DC, Lieber CM (2002) Nature 415:617
11. Le Loarer J-L, Nussbaum H, Bortzmeyer D (1998) Alumina extrudates, methods for preparing and use as catalysts or catalyst supports. Rhodia Chimie, France. Application: WO, p 44
12. Burkat VS, Dudorova VS, Smola VS, Chagina TS (1985) Light metals. TMS, Warrendale, PA, pp 1443–1448
13. Nedez C, Boitiaux J-P, Cameron CJ, Didillon B (1996) Langmuir 12:3927
14. Chen Y, Jin L, Xie Y (1998) J Sol-Gel Sci Technol 13:735
15. Xue DS, Huang YL, Ma Y, Zhou PH, Niu ZP, Li FS, Job R, Fahrner WR (2003) J Mater Sci Lett 22:1817
16. Philipse AP, Nechifor A-M, Patmamanoharan C (1994) Langmuir 10:4451
17. Okada K, Tanaka A, Hayashi S, Daimon K, Otsuka N (1994) J Mater Res 9:1709
18. Ananthakumar S, Raja V, Warrier KGK (2000) Mater Lett 43:174
19. van Bruggen MPB (1998) Langmuir 14:2245
20. Bugosh J (1961) J Phys Chem 65:1789
21. Kaya C, He JY, Gu X, Butler EG (2002) Microporous Mesoporous Mater 54:37
22. Kuang D, Fang Y, Liu H, Frommen C, Fenske D (2003) J Mater Chem 13:660
23. Zhu HY, Gao XP, Song DY, Bai YQ, Ringer SP, Gao Z, Xi YX, Martens W, Riches JD, Frost RL (2004) J Phys Chem B 108:4245
24. Zhu HY, Riches JD, Barry JC (2002) Chem Mater 14:2086
25. Wood L, Lindley J (1980) Liquid phase chemical process with separation of catalyst particles by magnetic flocculation. Imperial Chemical Industries Ltd., UK. Application: EP, p 21
26. Teunissen W, Bol AA, Geus JW (1999) Catal Today 48:329
27. Zhu HY, Gao XP, Song DY, Bai YQ, Ringer SP, Gao Z, Xi YX, Martens W, Riches JD, Frost RL (2004) J Phys Chem B 108:4245
28. Gao P, Xie Y, Chen Y, Ye L, Guo Q (2005) J Cryst Growth 285:555
29. Shen SC, Chen Q, Chow PS, Tan GH, Zeng XT, Wang Z, Tan RBH (2007) J Phys Chem C 111:700
30. Frost RL, Vassallo AM (1996) Clays Clay Miner 44:635
31. Frost RL, Vassallo AM (1997) Mikrochim Acta Suppl 14:789
32. Frost RL, Kloprogge JT (1999) Spectrochim Acta A 55A:2195
33. Frost RL, Weier ML (2003) Thermochim Acta 406:221
34. Zhao Y, Frost RL (2008) J Colloid Interf Sci 326:289
35. Cummins PG, Hayter JB, Penfold J, Staples E (1987) Chem Phys Lett 138:436
36. Cummins PG, Staples E, Penfold J, Heenan RK (1989) Langmuir 5:1195
37. Kahlweit M (1970) Physical chemistry. Academic Press, New York